

# UC San Diego

## UC San Diego Previously Published Works

### Title

Significant age-related differences between lower leg muscles of older and younger female subjects detected by ultrashort echo time magnetization transfer modeling

### Permalink

<https://escholarship.org/uc/item/609892vf>

### Journal

NMR in Biomedicine, 37(12)

### ISSN

0952-3480

### Authors

Jerban, Saeed

Mohammadi, Hamidreza Shaterian

Athertya, Jiyo S

et al.

### Publication Date

2024-12-01




### DOI

10.1002/nbm.5237

Peer reviewed

## RESEARCH ARTICLE

# Significant age-related differences between lower leg muscles of older and younger female subjects detected by ultrashort echo time magnetization transfer modeling

Saeed Jerban<sup>1</sup> | Hamidreza Shaterian Mohammadi<sup>1</sup>  | Jiyo S. Athertya<sup>1</sup>  | Amir Masoud Afsahi<sup>1</sup> | Niloofar Shojaeiadib<sup>1</sup> | Dina Moazamian<sup>1</sup>  | Samuel R. Ward<sup>2</sup> | Gina Woods<sup>3</sup> | Christine B. Chung<sup>1,4</sup> | Jiang Du<sup>1,4</sup> | Eric Y. Chang<sup>1,4</sup>

<sup>1</sup>Department of Radiology, University of California, San Diego, CA, USA

<sup>2</sup>Department of Orthopaedic Surgery, University of California San Diego, San Diego, CA, USA

<sup>3</sup>Department of Medicine, University of California, San Diego, CA, USA

<sup>4</sup>Research Service, Veterans Affairs San Diego Healthcare System, San Diego, CA, USA

## Correspondence

Eric Y. Chang, Radiology Service, Veterans Affairs San Diego Healthcare System, 3350 La Jolla Village Drive, San Diego, CA 92161, USA.  
Email: [eric.chang2@va.gov](mailto:eric.chang2@va.gov)

Saeed Jerban and Hamidreza Shaterian Mohammadi, Department of Radiology, University of California, 9500 Gilman Dr., San Diego, CA 92093, USA.

Email: [sjerban@health.ucsd.edu](mailto:sjerban@health.ucsd.edu)  
Email: [hmohammadi@health.ucsd.edu](mailto:hmohammadi@health.ucsd.edu)

## Funding information

National Institutes of Health, Grant/Award Numbers: K01AR080257, R01AR068987, R01AR062581, R01AR075825, 5P30AR073761, F32AG082458; Veterans Affairs R&D, Grant/Award Numbers: I01CX001388, I01BX005952, I01CX000625; GE Healthcare

## Abstract

Magnetization transfer (MT) magnetic resonance imaging (MRI) can be used to estimate the fraction of water and macromolecular proton pools in tissues. MT modeling paired with ultrashort echo time acquisition (UTE-MT modeling) has been proposed to improve the evaluation of the myotendinous junction and fibrosis in muscle tissues, which the latter increases with aging. This study aimed to determine if the UTE-MT modeling technique is sensitive to age-related changes in the skeletal muscles of the lower leg. Institutional review board approval was obtained, and all recruited subjects provided written informed consent. The legs of 31 healthy younger ( $28.1 \pm 6.1$  years old,  $BMI = 22.3 \pm 3.5$ ) and 20 older ( $74.7 \pm 5.5$  years old,  $BMI = 26.7 \pm 5.9$ ) female subjects were imaged using UTE sequences on a 3 T MRI scanner. MT ratio (MTR), macromolecular fraction (MMF), macromolecular T2 (T2-MM), and water T2 (T2-W) were calculated using UTE-MT modeling for the anterior tibialis (ATM), posterior tibialis (PTM), soleus (SM), and combined lateral muscles. Results were compared between groups using the Wilcoxon rank sum test. Three independent observers selected regions of interest (ROIs) and processed UTE-MRI images separately, and the intraclass correlation coefficient (ICC) was calculated for a reproducibility study. Significantly lower mean MTR and MMF values were present in the older compared with the younger group in all studied lower leg muscles. T2-MM showed significantly lower values in the older group only for PTM and SM muscles. In contrast, T2-W showed significantly higher values in the older group. The age-related differences were more pronounced for MMF ( $-17$  to  $-19\%$ ) and T2-W ( $+20$  to  $47\%$ ) measurements in all muscle groups compared with other investigated MR measures. ICCs were higher than 0.93, indicating excellent consistency between

**Abbreviations:** ATM, anterior tibialis muscle; BMI, body mass index; DT, diffusion tensor; ICC, intraclass correlation coefficient; IRB, institutional review board; K, proton exchange rate; LM, lateral muscle; MM, macromolecular; MMF, macromolecular fraction; MRI, magnetic resonance imaging; MSK, musculoskeletal; MT, magnetization transfer; MTR, magnetization transfer ratio;  $M_{0M}$ , fully relaxed magnetization of the macromolecular pool;  $M_{0W}$ , fully relaxed magnetization of the water pool; PTM, posterior tibialis muscle; RF, radiofrequency; ROI, regions of interest;  $R_{1M}$ , macromolecular pool;  $R_{1W}$ , longitudinal relaxation rate of the water pool; SM, soleus muscle; T1, spin-lattice relaxation time; T2, spin-spin relaxation time; T2-MM, macromolecular T2; T2-W, water T2; TE, echo time; TR, repetition time; UTE, ultrashort echo time.

Saeed Jerban and Hamidreza Shaterian Mohammadi equally contributed to this research work.

the ROI selection and MRI measurements of independent readers. As demonstrated by significant differences between younger and older groups, this research emphasizes the potential of UTE-MT MRI techniques in evaluating age-related skeletal muscle changes.

#### KEYWORDS

macromolecular protons, magnetization transfer, MRI, muscle, myotendinous junction, UTE

## 1 | INTRODUCTION

Magnetic resonance imaging (MRI) is a comprehensive imaging modality to assess skeletal muscle quality and quantity<sup>1–3</sup>. Muscle injuries and other pathologies may be observed on MRI, including inflammation, fat infiltration, fibrosis, and atrophy. Several conventional MRI techniques are routinely utilized for morphological muscle assessments, such as spin–lattice (T1)-weighted, spin–spin (T2)-weighted<sup>2,4</sup>, and short-tau-inversion-recovery<sup>5,6</sup> imaging. However, the standard qualitative morphological MRI-based muscle assessments are subjective and may lack reproducibility. On the other hand, quantitative MRI techniques have been proposed to provide more sensitive, objective, and reproducible measures of the muscle microstructure and composition. T1 and T2 relaxation times<sup>2,3,7–13</sup>, magnetization transfer (MT) related measures<sup>12–21</sup>, chemical exchange saturation transfer (CEST) measures<sup>22,23</sup>, diffusion tensor (DT) indices<sup>23,24–27</sup>, and water-fat separation<sup>23,28–37</sup> techniques are the most reported quantitative MRI techniques in the literature.

Among the abovementioned quantitative MRI techniques, MT can provide information on proton pools, such as water and macromolecules, of which the latter is not directly detectable with current MRI techniques and hardware. Notably, the direct imaging and quantification of macromolecules, which have only a few microseconds T2s, require MR imaging at echo times (TEs) of around one microsecond. MT ratio or relative volume estimations of the pools (e.g., macromolecular fraction, MMF)<sup>14,15,21</sup> are common MT measures used in the musculoskeletal (MSK) system. In skeletal muscle, the myofibrillar proteins and collagen are the dominant macromolecules, and a measurement of the macromolecular pool could be potentially sensitive to the muscle quality and its ability to generate force<sup>38–40</sup>. With MT techniques, a high-power saturation radiofrequency (RF) pulse is used with a predefined frequency offset apart from the known resonance frequency of water to saturate mainly protons in macromolecules. Then, the saturated magnetization transfers from the macromolecules to the water protons, which can be demonstrated by MRI as a reduction in signal intensity.

MT imaging combined with ultrashort echo time (UTE) MRI has been used to evaluate macromolecular contents in several biological tissues<sup>41,42</sup>. Regarding the evaluation of the myotendinous junction and fibrotic regions in the skeletal muscles, UTE-MT modeling may be particularly helpful. Specifically, signal detection in these tissues is challenging, and they demonstrate low signal with conventional MRI sequences that utilize TEs above a few milliseconds. The low detectable signal in these tissues is likely caused by short T2 values and higher bound water concentration, which has not been investigated thoroughly. Remarkably, UTE-MT modeling has been shown to be insensitive to tissue orientation (i.e., the so-called “magic angle effect”) and to provide a robust assessment of MSK tissues regardless of their orientation within the MRI scanner<sup>43</sup>.

UTE-MT modeling was previously used to detect differences between tendons of healthy young and old subjects<sup>44</sup>, which are likely related to compositional and structural changes<sup>43,45</sup> through the aging process. However, the age-related differences in muscle remain to be investigated. The decline in skeletal muscle mass and function has been consistently observed with aging. Aging muscle exhibits a diverse set of characteristics, including heterogeneous muscle fiber atrophy, muscle fiber loss, reconfiguration of the spatial arrangement of muscle fibers within motor units, and a progressive rise in non-contractile adipose and fibrotic tissues<sup>46–48</sup>. If UTE-MT modeling is sensitive to the changes with aging in skeletal muscle, it may help monitor the microstructural changes in patients suffering from sarcopenia. The main objective of this study was to determine if UTE-MT modeling is sensitive to age-related changes in human lower-leg muscles.

## 2 | MATERIAL AND METHODS

The institutional review board (IRB) of the University of California, San Diego, approved this study. This study followed applicable good clinical practice requirements and the relevant guidelines and regulations. Written informed consent was obtained from subjects prior to participation.

### 2.1 | Subject recruitment

Two female cohorts were recruited, including younger, healthy subjects under 45 years of age and healthy postmenopausal subjects over 50 years of age. Subjects in the former group were required not to be pregnant, and subjects in the latter group were required to have had a bone

densitometry scan within the past year confirming the absence of osteoporosis. In total, 31 healthy younger female subjects ( $28.1 \pm 6.1$  years old, BMI =  $22.3 \pm 3.5$ ) and 20 older female subjects ( $74.7 \pm 5.5$  years old, BMI =  $26.7 \pm 5.9$ ) were recruited.

## 2.2 | UTE-MRI scanning protocol

The subjects' lower legs were imaged using UTE-MRI sequences on a 3 T MRI scanner (MR750, GE Healthcare Technologies, WI, USA) employing a standard eight-channel knee coil. Eighteen and seven subjects selected the right leg to be scanned in younger and older groups, respectively. The imaging slab was centered in the middle of the tibia based on anatomical landmarks. A 3D-UTE-Cones-MT sequence (Fermi saturation pulse power =  $500^\circ$ ,  $1000^\circ$ , and  $1500^\circ$ ; frequency offset = 2, 5, 10, 20, and 50 kHz; FA =  $7^\circ$ ; 9 spokes per MT preparation; rectangular RF excitation pulse of 100  $\mu$ s) was performed for two-pool MT modeling.<sup>1,2</sup> Field of view, matrix dimension, in-plane pixel size, slice thickness, and total scan time were 14 cm,  $160 \times 160$ ,  $0.87 \times 0.87$  mm<sup>2</sup>, 5 mm, and 15 min, respectively. A non-UTE cones sequence (TR = 100, TE = 2.2 ms) was also performed to provide a high-contrast image for selecting regions of interest (ROIs).

## 2.3 | MRI data analysis

An open-source software (Elastix, <http://elastix.isi.uu.nl/>) was used to register (the images from all MT acquisitions to the non-UTE cones image via intensity-based rigid registration to compensate for the potential subject motion between sequences. A Gaussian filter was performed within  $3 \times 3$ -pixel sub-windows to smooth images slightly before further measurements.

ROIs were selected by three experienced MRI observers at the four following muscles: anterior tibialis muscle (ATM), posterior tibialis muscle (PTM), soleus muscle (SM), and combined lateral muscles (LM, including the peroneus longus and the extensor digitorum longus muscles). The ROIs were selected in one axial slice in the middle of the lower leg (also in the middle of the scanning coverage, 120 mm long. Tendons and aponeuroses were avoided. Figure 1A and B shows representative ROIs for ATM, PTM, SM, and LM (yellow dashed line) selected by one of the observers on axial images of the lower leg using the Cones UTE-MRI sequence and Cones at TE = 2.2 ms. All observers followed the same method for ROI selection, shown in Figure 1. For quality control purposes, the selected ROIs by the observers were overseen and validated by a board-certified MSK radiologist for the first three datasets.

Average magnetization transfer ratio (MTR) within ROIs for different MT saturation pulse powers ( $500^\circ$ ,  $1000^\circ$ , and  $1500^\circ$ ) and frequency offsets (2, 5, 10, 20, and 50 kHz) were calculated from the raw images. Average macromolecular proton fraction (MMF), macromolecular T2 (T2-MM), and water T2 (T2-W) were calculated for all the selected ROIs using the MT modeling. In this model, the muscle tissue is assumed to have two different proton pools (two-pool model). The first pool is a macromolecular proton pool, comprised of the protons in the myofibrillar proteins and collagen fibers, which has a broad spectrum of extremely short T2 ( $\sim 10$   $\mu$ s). The second pool is the total water proton pool, which has a narrow spectrum of much higher T2 and includes protons in free water and bound water to the muscle fibers. The protons of the two pools are continuously exchanging their magnetizations. When the off-resonance saturation pulse is applied in our acquisition, the macromolecular

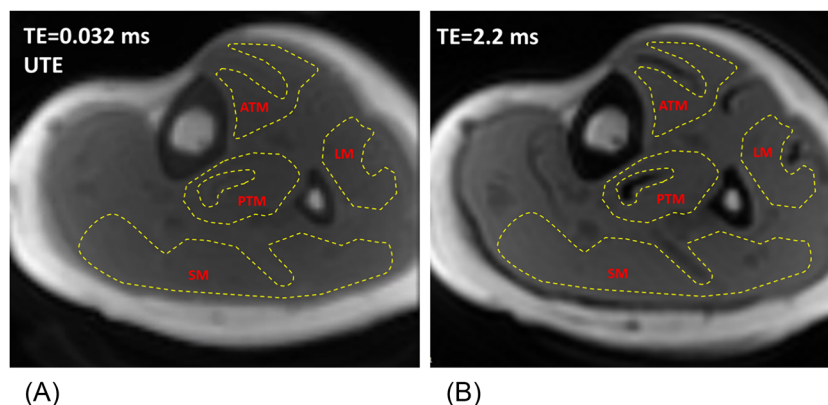


**FIGURE 1** Representative axial images of the lower leg of a healthy 31-year-old female participant using (A) ultrashort echo time (UTE) cones MRI sequence (TE = 0.032 ms) and (B) cones MRI sequence at TE = 2.2 ms. Representative regions of interest (ROIs, indicated by yellow dashed boundaries) for anterior tibialis muscle (ATM), posterior tibialis muscle (PTM), soleus muscle (SM), and combined lateral muscles (LM, including peroneus longus and extensor digitorum longus) were first selected at TE = 2.2 ms because it provided higher contrast, and then overlaid on the UTE images.

proton magnetization is partially saturated, then the saturation transfers to the water pool, and eventually, the acquired water signal intensity decreases because of the magnetization transfer. A two-pool MT model is built based on the Bloch equation, such that the saturated signal in UTE-MT acquisition is defined as a function of MMF and the following MR properties of both pools: a) fully relaxed magnetization of the macromolecular pool ( $M_{0M}$ ) and water pool ( $M_{0W}$ ), b) the longitudinal relaxation rate constants of the macromolecular pool ( $R_{1M}$ ) and water pool ( $R_{1W}$ ), c) the proton exchange rate constant between the two pools ( $K$ ), and d) the loss rate of longitudinal magnetization of the macromolecular pool<sup>38</sup>. A super-Lorentzian line shape was used to model the macromolecular proton spectrum and the loss of the longitudinal magnetization of the macromolecular pool<sup>38</sup>. To avoid long scan time, T1 values were not measured in this study. A T1 of 1000 ms ( $R_{1W} = 0.001$ ) was used as the input for the MT modeling, which was in the range of previously published values<sup>12,21</sup>, resulting in less sensitivity in MMF values (supplemental figure, Jerban et al.<sup>21</sup>).

The ROI selection and UTE-MT analysis were performed offline on the DICOM images using an in-house code written in MATLAB (version 2017, Mathworks, Natick, MA, USA).

## 2.4 | Statistical analysis

All statistical analyses were performed using MATLAB software. The UTE-MT modeling results (MMF, T2-MM, and T2-W) and MTRs were compared between younger and older groups using a two-sided Wilcoxon rank sum test, which is appropriate for unequal sample size and non-normal data distributions (tested by One-sample Kolmogorov–Smirnov test).  $p$ -Values  $<0.05$  were considered significant. The significance level for multiple comparisons was corrected using the Holm–Bonferroni method.

To investigate the reproducibility of the data analysis steps, the intraclass correlation coefficient (ICC) was calculated between MRI measures performed by the three independent observers.

## 3 | RESULTS

Figure 2 shows the UTE-MT modeling curves performed in ATM of representative subjects in younger and older groups. The three pulse saturation powers are indicated with different color lines ( $1500^\circ$  in red,  $1000^\circ$  in green, and  $500^\circ$  in blue) which each was performed at five different frequency offsets (2, 5, 10, 20, and 50 kHz). In this example of ATM muscle, MMF was lower, but T2-MM and T2-W were higher in the representative older subject.

Table 1 presents the mean and standard deviation values of MTR, MMF, T2-MM, and T2-W in the four investigated lower muscles for younger and older groups. Independent measurements by the three observers were averaged. ICC between the three independent measurements was higher than 0.93 for MTRs and 0.96 for MT modeling measures, which indicates excellent consistency between measurements performed by independent observers. The 15 MTR values calculated from the raw data showed similar trends; therefore, only MTRs at 2 kHz frequency offset for 1000 and 1500 pulse power levels are presented in Table 1, which have higher values in general.

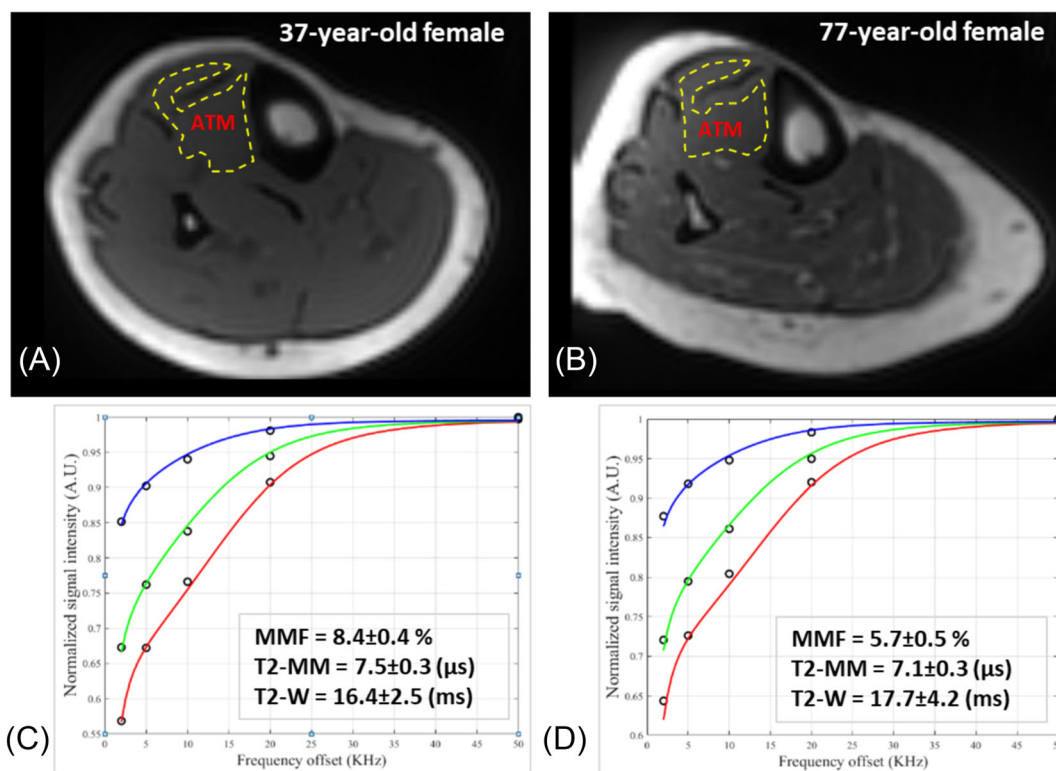
Average percentage differences in MTRs and UTE-MT modeling results between younger and older groups, as well as the Wilcoxon rank sum test significance, are presented in Table 2. After correcting the significance level for multiple comparisons, MTRs and MMF were found to be significantly lower on average in the older group than the younger group in all studied muscles. T2-MM showed significantly lower values in the older group only for PTM and SM muscles. In contrast, T2-W showed significantly higher values in the older group. The age-related differences were more pronounced for MMF ( $-17$  to  $-19\%$ ) and T2-W ( $+20$  to  $47\%$ ) measurements in all muscle groups compared with other investigated MR measures.

Figure 3 shows boxplots of the MRI results for the younger and older groups. Boxplots visualize the MRI measure differences between groups, showing the well-pronounced decreasing pattern in MTRs and MMF while increasing the pattern in T2-W by aging. As can be found from the larger SD and the range in the boxplot, the MR measures showed higher variations in the older group.

## 4 | DISCUSSION

This study highlights the potential of the two-pool UTE-MT modeling technique for non-invasive skeletal muscle assessment and detecting age-related differences. Aging generally affects the quality, composition, and performance of the muscles<sup>40</sup>. UTE-MT modeling is hypothesized to detect collagen fraction changes throughout aging.

The MMF of all the lower-leg muscles in this study was found to be significantly lower in the older group than in young subjects. MMF reduction most likely indicates a lower macromolecular content, likely dominant by myofibrillar fiber decline, in the skeletal muscles, although increases in water content can also contribute. The estimated water T2 in the studied muscles was significantly higher in the older group. Since using UTE



**FIGURE 2** Two-pool UTE-MT modeling in ATM muscle of representative subjects from the younger and older groups. Representative axial images of the lower leg (cones MRI sequence at TE = 2.2 ms) of a healthy (A) 37-year-old female and (B) 77-year-old female. Schematics of the selected ROIs for ATM muscle are indicated in yellow dashed boundaries. The two-pool MT modeling curves for the ATM muscle of the (C) healthy younger and (D) older subjects using three pulse saturation powers (1500° in red, 1000° in green, and 500° in blue) and five frequency offsets (2, 5, 10, 20, and 50 kHz). MMF was lower but T2-MM and T2-W were higher in the representative older subject. **MMF**: macromolecular fraction, **T2-MM**: macromolecular T2 and **T2-W**: water T2.

**TABLE 1** UTE-MT measurements in four lower leg muscles and intraclass correlation coefficients (ICC) between the three independent observers.

		MTR-15-2 <sup>a</sup> (%)	MTR-10-2 <sup>a</sup> (%)	MMF (%)	T2-MM (μs)	T2-W (ms)
ATM	Younger	43.2 ± 2.2	33.2 ± 2.4	9.3 ± 2.5	7.5 ± 0.3	14.9 ± 2.9
	Older	40.0 ± 3.6	30.1 ± 3.1	7.5 ± 1.7	7.4 ± 0.3	17.9 ± 5.0
PTM	Younger	42.6 ± 2.2	32.5 ± 2.4	9.2 ± 2.6	7.5 ± 0.3	14.4 ± 2.4
	Older	39.3 ± 2.8	29.5 ± 2.8	7.6 ± 1.7	7.3 ± 0.4	18.1 ± 4.5
SM	Younger	42.2 ± 1.8	32.3 ± 1.9	9.0 ± 2.3	7.4 ± 0.3	16.8 ± 3.4
	Older	37.8 ± 4.8	28.3 ± 4.0	7.4 ± 1.9	7.2 ± 0.4	24.8 ± 6.0
LM	Younger	43.1 ± 2.1	33.1 ± 2.4	9.3 ± 2.4	7.4 ± 0.3	16.3 ± 3.6
	Older	39.6 ± 3.3	29.8 ± 3.0	7.6 ± 1.8	7.2 ± 0.4	20.3 ± 5.4
Mean	Younger	42.8 ± 1.9	32.8 ± 2.2	9.2 ± 2.4	7.4 ± 0.3	15.6 ± 2.9
	Older	39.2 ± 3.4	29.4 ± 3.0	7.5 ± 1.7	7.3 ± 0.3	20.3 ± 7.5
ICC		0.98 ± 0.02	0.98 ± 0.02	0.93 ± 0.02	0.97 ± 0.01	0.95 ± 0.02

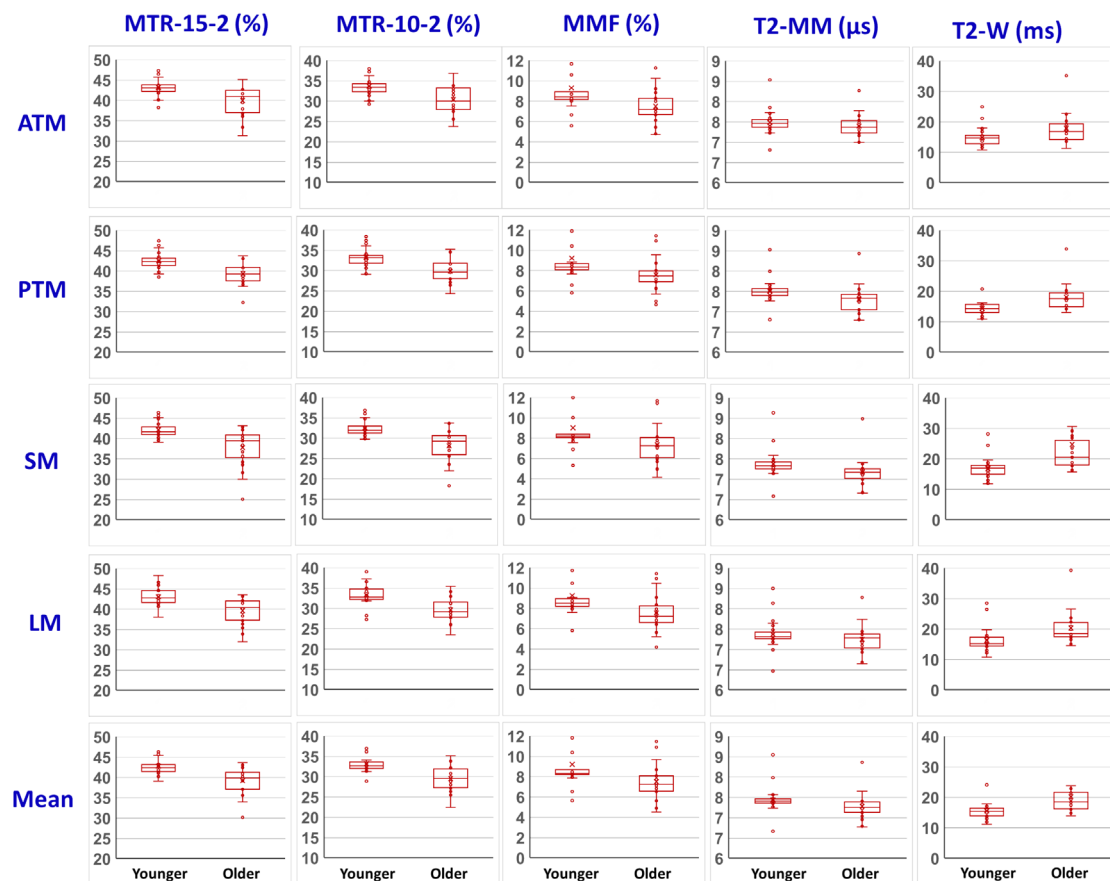
<sup>a</sup>MTR-15-2 and MTR-10-2 refer to magnetization ratio at 2 kHz frequency offset for 1500 and 1000° pulse power levels, respectively. **ATM**: anterior tibialis, **ICC**: intraclass correlation coefficient, **LM**: lateral muscle, **MMF**: macromolecular fraction, **MTR**: Magnetization transfer ratio, **PTM**: posterior tibialis muscle, **SM**: soleus muscle, **T2-MM**: macromolecular T2 and **T2-W**: water T2.

MR acquires both bound and free water signals, a higher T2-W in the older group might indicate expanding free water volume, or a shrinking macromolecular-bound water pool related to advancing age. Additionally, a higher fraction of microscopic intramuscular fat within the studied muscles of the older group could also explain the lower MMF and MTR values while higher T2-W. Previous investigation has shown that including

**TABLE 2** Differences between UTE-MT measures of older and younger lower leg muscles (in percentage).

	Older-younger difference (%)				
	MTR-15-2 <sup>a</sup>	MTR-10-2 <sup>a</sup>	MMF	T2-MM	T2-W
<b>ATM</b>	-7.47 ( <i>p</i> = 0.001)	-9.35 ( <i>p</i> = 0.002)	-19.28 ( <i>p</i> = 0.002)	-1.16 ( <i>p</i> = 0.115)	20.44 ( <i>p</i> = 0.007)
<b>PTM</b>	-7.66 ( <i>p</i> = 0.001)	-9.20 ( <i>p</i> = 0.001)	-17.62 ( <i>p</i> = 0.001)	-2.64 ( <i>p</i> = 0.001)	25.25 ( <i>p</i> < 0.001)
<b>SM</b>	-10.47 ( <i>p</i> < 0.001)	-12.33 ( <i>p</i> < 0.001)	-18.24 ( <i>p</i> = 0.001)	-2.64 ( <i>p</i> < 0.001)	47.43 ( <i>p</i> < 0.001)
<b>LM</b>	-8.13 ( <i>p</i> < 0.001)	-9.98 ( <i>p</i> < 0.001)	-18.48 ( <i>p</i> = 0.001)	-1.73 ( <i>p</i> = 0.115)	25.03 ( <i>p</i> < 0.001)
<b>Mean</b>	-8.42 ( <i>p</i> < 0.001)	-10.21 ( <i>p</i> < 0.001)	-18.41 ( <i>p</i> = 0.001)	-2.04 ( <i>p</i> = 0.003)	30.02 ( <i>p</i> < 0.001)

<sup>a</sup>MTR-15-2 and MTR-10-2 refer to magnetization ratio at 2 kHz frequency offset for 1500 and 1000° pulse power levels, respectively. **ATM**: anterior tibialis, **LM**: lateral muscle, **MMF**: macromolecular fraction, **MTR**: Magnetization transfer ratio, **PTM**: posterior tibialis muscle, **SM**: soleus muscle, **T2-MM**: macromolecular T2 and **T2-W**: water T2.

**FIGURE 3** Boxplots of MTR, MMF, T2-MM, and T2-W within the selected muscles for younger and older groups. Mean, SD, first, and third quartile values are indicated in the boxplots.

large fatty regions in the muscle of interest can result in lower MMF and MTR in calculations<sup>21</sup>. It should be noted that the MTR, MMF, and T2-W exhibited higher variation in the older group than the younger group, likely due to greater heterogeneity in age-related changes.

The estimated muscle MMF and T2-MM in this study were in the range of previously reported values in the literature<sup>14,49</sup>. Notably, quantitative MT modeling has not been reported in the literature to be used for the assessment of age-related differences in muscle. The estimated T2-W



in this study was lower than the reported values in the literature for skeletal muscles using different fitting methods<sup>2,50–52</sup>, likely due to missing a major portion of the protons with short T2 (short component) by acquiring the MR images at much longer echo times.

UTE-MT modeling has been previously shown to be insensitive to tissue orientation and may thus provide a more robust assessment of anisotropic MSK tissues compared with techniques that are sensitive to the so-called “magic angle effect,” where values may differ relative to tissue orientation within the MRI scanner<sup>41,43</sup>. The T2 and regular T1 $\rho$  are two examples of the orientation-sensitive MRI methods. UTE-MT has also been shown to be less sensitive to macroscopic fat replacement if a correct T1 value is used in the modeling, suggesting the use of lower T1 values when large fat infiltrations are obvious in the muscle of interest<sup>21</sup>. The UTE-MT technique may be a useful tool for muscle assessment, particularly near the myotendinous junction or in conditions where fibrosis occurs, which shortens the T2 of the tissues. It should be noted that UTE-MT modeling has been previously used mainly to assess MSK tissues with higher fractions of short T2 components compared with skeletal muscle, such as in cartilage<sup>53,54</sup>, meniscus<sup>53</sup>, ligament<sup>55</sup>, tendon<sup>44,56–59</sup>, and bone<sup>60–64</sup>. In our previous study of tibialis tendons through the aging process<sup>44</sup>, MMF demonstrated significantly lower values on average in the elderly group compared with the younger group for both anterior (lower by 16.8%,  $p = 0.03$ ) and posterior tibialis (lower by 23.0%,  $p < 0.01$ ), which are in the range of observed differences for tibialis muscle in this study. Other parameters from UTE-MT modeling in tibialis tendons did not show a significant nor a consistent difference between the young and elderly groups.

Although the mean signal within the targeted muscles was used in this study for UTE-MT modeling and provided mean values, pixel maps of the UTE-MT-related markers can also be achieved potentially demonstrating local variations within the muscles, which may be of interest to investigators in future studies. Figure 4 shows the pixel maps of MTR, MMF, T2-MM, and T2-W in an axial slice of the lower leg muscles of a representative subject from the younger group (37-year-old female) and a representative subject from the older group (77-year-old female).

Several other quantitative MRI techniques for muscle assessments have been reported in the literature. T1 and T2 measurements have been used for muscle injury and pathology assessment and aging-related differences in several investigations<sup>7–10,12</sup>. Briefly, T1 values were found to be higher in muscle inflammation regions, while they are lower in fat-infiltrated regions<sup>7</sup>. T2 values, however, are found to be higher in both muscle inflammation and fat-infiltrated regions<sup>11</sup>. Diffusion MRI has been widely used to evaluate the diffusion preference directions by the water molecules in tissues with well-organized fibers such as muscles, tendons, and ligaments. Diffusion indices can provide information about the tissue microstructure and fibers' orientation at a microscopic level. The diffusion properties of muscle, especially the third eigenvalue of the diffusion tensor and degree of diffusion anisotropy, reflect muscle damage due to experimental injury<sup>27</sup>, strain injury<sup>26</sup>, and disease<sup>24,25</sup>. Moreover, since macroscopic fat infiltration is a widespread observation in muscle pathologies and injuries, several studies have been devoted to performing an accurate estimation of the fat content in tissues, most employing the different frequencies of fat and water protons<sup>28–37</sup>.

Other quantitative MRI techniques have also been used to investigate age-related changes in human lower leg skeletal muscles. In summary, muscle T2 and T1 have been reported to increase by aging in several investigations<sup>12,65–67</sup>. T2 reduction was observed in the current study as well for both macromolecular and water components of the investigated muscles. Fat fraction in muscle has been reported to be increasing with aging in the literature<sup>65–67</sup>, which has not been investigated in the current study. MTR and MT Saturation have been reported to decrease by aging<sup>12,66,67</sup>, which is consistent with the findings in the current study. DT imaging has been also used to investigate the age-related changes in muscle, that shows a decline in mean diffusivity yet an increase in fractional anisotropy of the muscles in several studies<sup>66,68</sup>.

The limitations of this study can be summarized in several aspects. First, the number of subjects was small, as is the nature of pilot studies. Second, we used 15 separate UTE-MT acquisitions for MT modeling, which made it necessary to perform image registration between image series for most of the subjects. The feasibility of using UTE-MT modeling with fewer data sets (e.g., two pulse power levels and frequency offsets) should be examined in future studies. Third, the impact of the intramuscular fat was not investigated in this study, which would affect the estimated MR properties, though the subjects in this study were healthy, and gross muscular atrophy was not observed. Performing muscle biopsies and comparisons with the standard image-based assessments and MR-based fat fraction estimations are required to examine the diagnostic application of the presented technique in muscle assessment. Additionally, the volume and size of the muscles are crucial parameters that should be combined with the presented compositional measures in this study when seeking correlations with the clinical outcomes. Fourth, this study only included female participants to avoid gender-related differences. Performing a similar study on male cohorts and comparing the results with the presented findings on female cohorts will be a future step. However, some studies have observed no significant differences in the sarcopenia prevalence rates between the older male and female populations<sup>69</sup>. Fifth, this investigation only included lower leg muscles, which may not be the main muscle sets determining the human ambulatory capacity or the most affected by aging. Future studies focused on other critical skeletal muscles, such as the thigh muscles in human ambulation, should be performed before confirming the capability of UTE-MT modeling in age-related muscle assessment. Sixth, only one axial slice was analyzed in this study. Therefore, the observed results may be slightly different if other slices or the complete volume of the muscles was included because of the potential heterogeneity in the studied muscles<sup>70,71</sup>. However, the impact of such heterogeneity on the age-related differences concluded here may be limited because of the consistent selection of the analyzed axial section in the middle of the lower leg. Moreover, the ROI selection for some of the investigated muscles in the study was not perfect and might suffer from overlaps with neighboring muscles because of the relatively low resolution of the UTE images and lack of morphological high-resolution images as a result of limited available scan time.



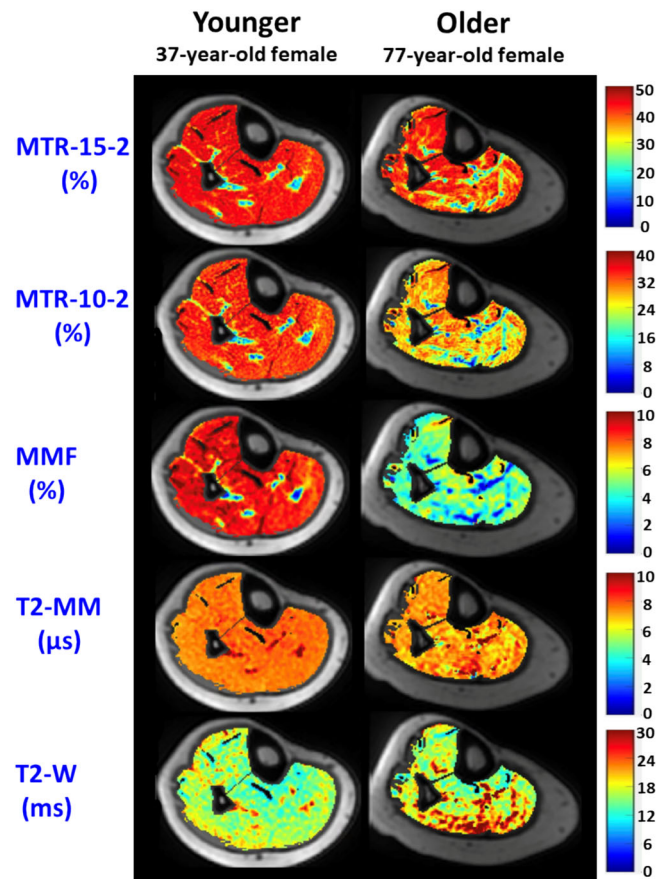


**FIGURE 4** Pixel maps of MTR, MMF, T2-MM, and T2-W in an axial slice of the lower leg within the selected muscles for younger and older groups.

## 5 | CONCLUSION

MTR and two-pool UTE-MT modeling were investigated for their capability to assess age-related changes in the human lower leg muscles. MMF obtained from MT modeling and MTRs showed significantly lower values, while T2-W demonstrated significantly higher values in the muscles of the older subjects compared with the younger group. This indicates compositional changes in skeletal muscles, likely related to the combination of the myofibrillar decline, free water increase, and intramuscular fat increase. MMF and T2-W differences between groups were higher than the MTR differences. This study highlights the utility of the UTE-MT MRI technique to assess skeletal muscles in the aging population, which may be used in the future for evaluating and monitoring sarcopenia patients.

### ACKNOWLEDGMENTS

The authors acknowledge grant support from the National Institutes of Health (K01AR080257, R01AR068987, R01AR062581, R01AR075825, 5P30AR073761, and F32AG082458), Veterans Affairs R&D (I01CX001388, I01BX005952, and I01CX000625), and GE Healthcare.

### CONFLICT OF INTEREST STATEMENT

The authors have no conflicts of interest to declare.

### DATA AVAILABILITY STATEMENT

The data that support the findings of this study are available from the corresponding author upon reasonable request.

### ORCID

Hamidreza Shaterian Mohammadi  <https://orcid.org/0009-0006-4749-437X>

Jiyo S. Athertya  <https://orcid.org/0000-0002-0866-1052>

Dina Moazamian  <https://orcid.org/0000-0002-8815-4535>

1. Guermazi A, Roemer FW, Robinson P, Tol JL, Regatte RR, Crema MD. Imaging of muscle injuries in sports medicine: sports imaging series. *Radiology*. 2017;282(3):646-663. doi:10.1148/radiol.2017160267
2. Hooijmans MT, Schlaefke L, Bolsterlee B, Schlaeger S, Marty B, Mazzoli V. Compositional and functional MRI of skeletal muscle: a review. *J Magn Reson Imaging*. 2024;60(3):860-877. doi:10.1002/jmri.29091
3. Engelke K, Chaudry O, Gast L, et al. Magnetic resonance imaging techniques for the quantitative analysis of skeletal muscle: state of the art. *J Orthop Translat*. 2023;42:57-72. doi:10.1016/j.jot.2023.07.005
4. Kaufman LD, Gruber BL, Gerstman DP, Kaell AT. Preliminary observations on the role of magnetic resonance imaging for polymyositis and dermatomyositis. *Ann Rheum Dis*. 1987;46(8):569-572. doi:10.1136/ard.46.8.569
5. Curiel RV, Jones R, Brindle K. Magnetic resonance imaging of the idiopathic inflammatory myopathies: structural and clinical aspects. *Ann N Y Acad Sci*. 2009;1154(1):101-114. doi:10.1111/j.1749-6632.2009.04386.x
6. Kimball AB, Summers RM, Turner M, et al. Magnetic resonance imaging detection of occult skin and subcutaneous abnormalities in juvenile dermatomyositis: implications for diagnosis and therapy. *Arthritis Rheum*. 2000;43(8):1866-1873. doi:10.1002/1529-0131(200008)43:8<3C1866::AID-ANR24%3E3.0.CO;2-6
7. Park JH, Olsen NJ Jr, King JL, et al. Use of magnetic resonance imaging and p-31 magnetic resonance spectroscopy to detect and quantify muscle dysfunction in the amyopathic and myopathic variants of dermatomyositis. *Arthritis Rheum*. 1995;38(1):68-77. doi:10.1002/art.1780380111
8. Huang Y, Majumdar S, Genant HK, et al. Quantitative MR relaxometry study of muscle composition and function in duchenne muscular dystrophy. *J Magn Reson Imaging*. 1994;4(1):59-64. doi:10.1002/jmri.1880040113
9. Kim HK, Laor T, Horn PS, Racadio JM, Wong B, Dardzinski BJ. T2 mapping in Duchenne muscular dystrophy: distribution of disease activity and correlation with clinical assessments. *Radiology*. 2010;255(3):899-908. doi:10.1148/radiol.10091547
10. Arpan I, Forbes SC, Lott DJ, et al. T2 mapping provides multiple approaches for the characterization of muscle involvement in neuromuscular diseases: a cross-sectional study of lower leg muscles in 5-15-year-old boys with Duchenne muscular dystrophy. *NMR Biomed*. 2013;26(3):320-328. doi:10.1002/nbm.2851
11. Fan RH, Does MD. Compartmental relaxation and diffusion tensor imaging measurements in vivo in  $\lambda$ -carrageenan-induced edema in rat skeletal muscle. *NMR Biomed*. 2008;21(6):566-573. doi:10.1002/nbm.1226
12. White JC, Sinha S, Sinha U. Spin lattice (T1) and magnetization transfer saturation (MTsat) imaging to monitor age-related differences in skeletal muscle tissue. *Diagnostics*. 2022;12(3):584. doi:10.3390/diagnostics12030584
13. Chen Y, Li L, Le N, Chang EY, Huang W, Ma YJ. On the fat saturation effect in quantitative ultrashort TE MR imaging. *Magn Reson Med*. 2022;87(5):2388-2397. doi:10.1002/mrm.29149
14. Sinclair CDJ, Samson RS, Thomas DL, et al. Quantitative magnetization transfer in in vivo healthy human skeletal muscle at 3 T. *Magn Reson Med*. 2010;64(6):1739-1748. doi:10.1002/mrm.22562
15. McDaniel JD, Ulmer JL, Prost RW, et al. Magnetization transfer imaging of skeletal muscle in autosomal recessive limb girdle muscular dystrophy. *J Comput Assist Tomogr*. 1999;23(4):609-614. doi:10.1097/00004728-199907000-00023
16. Bajd F, Škrlep M, Čandek-Potokar M, Vidmar J, Serša I. Application of quantitative magnetization transfer magnetic resonance imaging for characterization of dry-cured hams. *Meat Sci*. 2016;122:109-118. doi:10.1016/j.meatsci.2016.08.001
17. Romero IO, Sinha U. Magnetization transfer saturation imaging of human calf muscle: reproducibility and sensitivity to regional and sex differences. *J Magn Reson Imaging*. 2019;50(4):1227-1237. doi:10.1002/jmri.26694
18. Li K, Dortch RD, Kroop SF, et al. A rapid approach for quantitative magnetization transfer imaging in thigh muscles using the pulsed saturation method. *Magn Reson Imaging*. 2015;33(6):709-717. doi:10.1016/j.mri.2015.03.003
19. Li K, Dortch RD, Brian Welch E, Bryant ND, Buck AKW, Park JH. Multi-parametric MRI characterization of healthy human thigh muscles at 3.0 T-relaxation, magnetization transfer, fat/water, and diffusion tensor imaging. *NMR Biomed*. 2014;27(9):1070-1084. doi:10.1002/nbm.3159
20. Nuñez-Peralta C, Montesinos P, Alonso-Jiménez A, et al. Magnetization transfer ratio in lower limbs of late onset Pompe patients correlates with intramuscular fat fraction and muscle function tests. *Front Neurol*. 2021;12:12. doi:10.3389/fneur.2021.634766
21. Jerban S, Ma Y, Tang Q, et al. Robust assessment of macromolecular fraction (MMF) in muscle with differing fat fraction using ultrashort Echo time (UTE) magnetization transfer modeling with measured T1. *Diagnostics*. 2023;13(5):876. doi:10.3390/diagnostics13050876
22. Kogan F, Haris M, Debrosse C, et al. In vivo chemical exchange saturation transfer imaging of creatine (CrCEST) in skeletal muscle at 3T. *J Magn Reson Imaging*. 2014;40(3):596-602. doi:10.1002/jmri.24412
23. Kogan F, Haris M, Singh A, et al. Method for high-resolution imaging of creatine in vivo using chemical exchange saturation transfer. *Magn Reson Med*. 2014;71(1):164-172. doi:10.1002/mrm.24641
24. Qi J, Olsen NJ, Price RR, Winston JA, Park JH. Diffusion-weighted imaging of inflammatory myopathies: polymyositis and dermatomyositis. *J Magn Reson Imaging*. 2008;27(1):212-217. doi:10.1002/jmri.21209
25. McMillan AB, Shi D, Pratt SJP, Lovering RM. Diffusion tensor MRI to assess damage in healthy and dystrophic skeletal muscle after lengthening contractions. *J Biomed Biotechnol*. 2011;2011:970726. doi:10.1155/2011/970726
26. Zaraiskaya T, Kumbhare D, Noseworthy MD. Diffusion tensor imaging in evaluation of human skeletal muscle injury. *J Magn Reson Imaging*. 2006;24(2):402-408. doi:10.1002/jmri.20651
27. Heemsker AM, Strijkers GJ, Drost MR, van Bochove GS, Nicolay K. Skeletal muscle degeneration and regeneration after femoral artery ligation in mice: monitoring with diffusion MR imaging. *Radiology*. 2007;243(2):413-421. doi:10.1148/radiol.2432060491
28. Glover GH. Multipoint Dixon technique for water and fat proton and susceptibility imaging. *J Magn Reson Imaging*. 1991;1(5):521-530. doi:10.1002/jmri.1880010504
29. Yu H, McKenzie CA, Shimakawa A, et al. Multiecho reconstruction for simultaneous water-fat decomposition and T2\* estimation. *J Magn Reson Imaging*. 2007;26(4):1153-1161. doi:10.1002/jmri.21090
30. Reeder SB, Wen Z, Yu H, et al. Multicoil Dixon chemical species separation with an iterative least-squares estimation method. *Magn Reson Med*. 2004;51(1):35-45. doi:10.1002/mrm.10675
31. Yu H, Shimakawa A, McKenzie CA, Brodsky E, Brittain JH, Reeder SB. Multiecho water-fat separation and simultaneous R\*2 estimation with multi-frequency fat spectrum modeling. *Magn Reson Med*. 2008;60(5):1122-1134. doi:10.1002/mrm.21737

32. Schlaeger S, Sollmann N, Zoffl A, et al. Quantitative muscle mri in patients with neuromuscular diseases—association of muscle proton density fat fraction with semi-quantitative grading of fatty infiltration and muscle strength at the thigh region. *Diagnostics*. 2021;11(6):1056. doi:[10.3390/diagnostics11061056](https://doi.org/10.3390/diagnostics11061056)
33. Grimm A, Meyer H, Nickel MD, et al. A comparison between 6-point Dixon MRI and MR spectroscopy to quantify muscle fat in the thigh of subjects with sarcopenia. *J Frailty Aging*. 2019;8(1):21-26. doi:[10.14283/jfa.2018.16](https://doi.org/10.14283/jfa.2018.16)
34. Ma J. A single-point Dixon technique for fat-suppressed fast 3D gradient-echo imaging with a flexible echo time. *J Magn Reson Imaging*. 2008;27(4):881-890. doi:[10.1002/jmri.21281](https://doi.org/10.1002/jmri.21281)
35. Jang H, Carl M, Ma Y, et al. Fat suppression for ultrashort echo time imaging using a single-point Dixon method. *NMR Biomed*. 2019;32(5):e4069. doi:[10.1002/nbm.4069](https://doi.org/10.1002/nbm.4069)
36. Jang H, Carl M, Ma Y, et al. Fat suppression for ultrashort Echo time imaging using a single point Dixon method. *NMR Biomed* 2019;32(5):e4069. doi:[10.1002/nbm.4069](https://doi.org/10.1002/nbm.4069)
37. Berglund J, Johansson L, Ahlström H, Kullberg J. Three-point Dixon method enables whole-body water and fat imaging of obese subjects. *Magn Reson Med*. 2010;63(6):1659-1668. doi:[10.1002/mrm.22385](https://doi.org/10.1002/mrm.22385)
38. Willingham TB, Kim Y, Lindberg E, Bleck CKE, Glancy B. The unified myofibrillar matrix for force generation in muscle. *Nat Commun*. 2020;11(1):3722. doi:[10.1038/s41467-020-17579-6](https://doi.org/10.1038/s41467-020-17579-6)
39. Haus JM, Carrithers JA, Carroll CC, Tesch PA, Trappe TA. Contractile and connective tissue protein content of human skeletal muscle: effects of 35 and 90 days of simulated microgravity and exercise countermeasures. *Am J Physiol*. 2007;293(4):R1722-7. doi:[10.1152/ajpregu.00292.2007](https://doi.org/10.1152/ajpregu.00292.2007).-We
40. Volpi E, Nazemi R, Fujita S. Muscle tissue changes with aging. *Curr Opin Clin Nutr Metab Care*. 2004;7(4):405-410. doi:[10.1097/01.mco.0000134362.76653.b2](https://doi.org/10.1097/01.mco.0000134362.76653.b2)
41. Ma Y, Shao H, Du J, Chang EY. Ultrashort echo time magnetization transfer (UTE-MT) imaging and modeling: magic angle independent biomarkers of tissue properties. *NMR Biomed*. 2016;29(11):1546-1552. doi:[10.1002/nbm.3609](https://doi.org/10.1002/nbm.3609)
42. Ma Y, Chang EY, Carl M, Du J. Quantitative magnetization transfer ultrashort echo time imaging using a time-efficient 3D multispoke cones sequence. *Magn Reson Med*. 2017;00(2):1-9. doi:[10.1002/mrm.26716](https://doi.org/10.1002/mrm.26716)
43. Zhu Y, Cheng X, Ma Y, et al. Rotator cuff tendon assessment using magic-angle insensitive 3D ultrashort echo time cones magnetization transfer (UTE-cones-MT) imaging and modeling with histological correlation. *J Magn Reson Imaging*. 2018;48(1):160-168. doi:[10.1002/jmri.25914](https://doi.org/10.1002/jmri.25914)
44. Jerban S, Ma Y, Namiranian B, et al. Age-related decrease in collagen proton fraction in tibial tendons estimated by magnetization transfer modeling of ultrashort echo time magnetic resonance imaging (UTE-MRI). *Sci Rep*. 2019;November;(9):17974. doi:[10.1038/s41598-019-54559-3](https://doi.org/10.1038/s41598-019-54559-3)
45. Ashir A, Ma Y, Jerban S, et al. Rotator cuff tendon assessment in symptomatic and control groups using quantitative MRI. *J Magn Reson Imaging*. 2020;52(3):864-872. doi:[10.1002/jmri.27115](https://doi.org/10.1002/jmri.27115)
46. Lenchik L, Mazzoli V, Cawthon PM, Hepple RT, Boutin RD. Muscle steatosis and fibrosis in older adults, from the AJR special series on imaging of fibrosis. *Am J Roentgenol* August. 2023;222(5):e2329742. doi:[10.2214/AJR.23.29742](https://doi.org/10.2214/AJR.23.29742)
47. Codari M, Zanardo M, di Sabato ME, et al. MRI-derived biomarkers related to sarcopenia: a systematic review. *J Magn Reson Imaging*. 2020;51(4):1117-1127. doi:[10.1002/jmri.26931](https://doi.org/10.1002/jmri.26931)
48. Tosato M, Marzetti E, Cesari M, et al. Measurement of muscle mass in sarcopenia: from imaging to biochemical markers. *Aging Clin Exp Res*. 2017;29(1):19-27. doi:[10.1007/s40520-016-0717-0](https://doi.org/10.1007/s40520-016-0717-0)
49. Li K, Dortch RD, Kroop SF, et al. A rapid approach for quantitative magnetization transfer imaging in thigh muscles using the pulsed saturation method. *Magn Reson Imaging*. 2015;33(6):709-717. doi:[10.1016/j.mri.2015.03.003](https://doi.org/10.1016/j.mri.2015.03.003)
50. Varghese J, Scandling D, Joshi R, et al. Rapid assessment of quantitative T1, T2, and T2\* in lower extremity muscles in response to maximal treadmill exercise. *NMR Biomed*. 2015;28(8):998-1008. doi:[10.1002/nbm.3332](https://doi.org/10.1002/nbm.3332)
51. Sharafi A, Chang G, Regatte RR. Bi-component T1ρ and T2 relaxation mapping of skeletal muscle in-vivo. *Sci Rep*. 2017;7(1):14115. doi:[10.1038/s41598-017-14581-9](https://doi.org/10.1038/s41598-017-14581-9)
52. Keene KR, Beenakker JM, Hooijmans MT, et al. T2 relaxation-time mapping in healthy and diseased skeletal muscle using extended phase graph algorithms. *Magn Reson Med*. 2020;84(5):2656-2670. doi:[10.1002/mrm.28290](https://doi.org/10.1002/mrm.28290)
53. Jerban S, Kasibhatla A, Ma Y, et al. Detecting articular cartilage and meniscus deformation effects using magnetization transfer ultrashort Echo time (MT-UTE) modeling during mechanical load application : ex vivo feasibility study. *Cartilage*. 2020;8(DEC):1-10;(1\_suppl):665S-673S. doi:[10.1177/1947603520976771](https://doi.org/10.1177/1947603520976771)
54. Namiranian B, Jerban S, Ma Y, et al. Assessment of mechanical properties of articular cartilage with quantitative three-dimensional ultrashort echo time (UTE) cones magnetic resonance imaging. *J Biomech*. 2020;113:110085. doi:[10.1016/j.jbiomech.2020.110085](https://doi.org/10.1016/j.jbiomech.2020.110085)
55. Jerban S, Hananouchi T, Ma Y, et al. Correlation between the elastic modulus of anterior cruciate ligament (ACL) and quantitative ultrashort echo time (UTE) magnetic resonance imaging. *J Orthop Res* January. 2022;40(10):2330-2339. doi:[10.1002/jor.25266](https://doi.org/10.1002/jor.25266)
56. Aria Ashir BS, Ma Y, Jerban S, et al. Rotator cuff tendon assessment in symptomatic and control groups using quantitative MRI. *J Magn Reson Imaging*. 2020;52(3):864-872. doi:[10.1002/jmri.27115](https://doi.org/10.1002/jmri.27115)
57. Jerban S, Ma Y, Afsahi AM, et al. Lower macromolecular content in tendons of female patients with osteoporosis versus patients with osteopenia detected by ultrashort Echo time (UTE) MRI. *Diagnostics*. 2022;12(5):1061. doi:[10.3390/diagnostics12051061](https://doi.org/10.3390/diagnostics12051061)
58. Jerban S, Ma Y, Afsahi AM, et al. Lower macromolecular content in tendons of female patients with osteoporosis versus patients with osteopenia detected by ultrashort Echo time (UTE) MRI. *Diagnostics*. 2022;12:1061. doi:[10.3390/diagnostics12051061](https://doi.org/10.3390/diagnostics12051061)
59. Malhi BS, Jang H, Malhi MS, Berry DB, Jerban S. Tendon evaluation with ultrashort echo time (UTE) MRI: a systematic review. *Front Musculoskelet Disord*. 2024;2:1324050. doi:[10.3389/fmscd.2024.1324050](https://doi.org/10.3389/fmscd.2024.1324050)
60. Jerban S, Ma Y, Wong JHHJH, et al. Ultrashort echo time magnetic resonance imaging (UTE-MRI) of cortical bone correlates well with histomorphometric assessment of bone microstructure. *Bone* 2019;123(December 2018):8-17. doi: [10.1016/j.bone.2019.03.013](https://doi.org/10.1016/j.bone.2019.03.013)
61. Jerban S, Ma Y, Dorte EW, et al. Assessing cortical bone mechanical properties using collagen proton fraction from ultrashort echo time magnetization transfer (UTE-MT) MRI modeling. *Bone Rep* 2019;8(2):100220. doi: [10.1016/j.bonr.2019.100220](https://doi.org/10.1016/j.bonr.2019.100220)
62. Jerban S, Ma Y, Wan L, et al. Collagen proton fraction from ultrashort echo time magnetization transfer (UTE-MT) MRI modelling correlates significantly with cortical bone porosity measured with micro-computed tomography (μCT). *NMR Biomed*. 2019;32(2):e4045. doi:[10.1002/nbm.4045](https://doi.org/10.1002/nbm.4045)

63. Jerban S, Ma Y, Li L, et al. Volumetric mapping of bound and pore water as well as collagen protons in cortical bone using 3D ultrashort Echo time cones MR imaging techniques. *Bone*. 2019;127(Oct):120-128. doi:[10.1016/j.bone.2019.05.038](https://doi.org/10.1016/j.bone.2019.05.038)
64. Jerban S, Ma Y, Nazaran A, et al. Detecting stress injury (fatigue fracture) in fibular cortical bone using quantitative ultrashort echo time-magnetization transfer (UTE-MT): an ex vivo study. *NMR Biomed*. 2018;31(11):e3994. doi:[10.1002/nbm.3994](https://doi.org/10.1002/nbm.3994)
65. Farrow M, Biglands J, Tanner SF, et al. The effect of ageing on skeletal muscle as assessed by quantitative MR imaging: an association with frailty and muscle strength. *Aging Clin Exp Res*. 2021;33(2):291-301. doi:[10.1007/s40520-020-01530-2](https://doi.org/10.1007/s40520-020-01530-2)
66. Morrow JM, Sinclair CDJ, Fischmann A, et al. Reproducibility, and age, body-weight and gender dependency of candidate skeletal muscle MRI outcome measures in healthy volunteers. *Eur Radiol*. 2014;24(7):1610-1620. doi:[10.1007/s00330-014-3145-6](https://doi.org/10.1007/s00330-014-3145-6)
67. Schwenzer NF, Martirosian P, Machann J, et al. Aging effects on human calf muscle properties assessed by MRI at 3 tesla. *J Magn Reson Imaging*. 2009;29(6):1346-1354. doi:[10.1002/jmri.21789](https://doi.org/10.1002/jmri.21789)
68. Cameron D, Reiter DA, Adelnia F, et al. Age-related changes in human skeletal muscle microstructure and architecture assessed by diffusion-tensor magnetic resonance imaging and their association with muscle strength. *Aging Cell*. 2023;22(7):e13851. doi:[10.1111/acer.13851](https://doi.org/10.1111/acer.13851)
69. Tay L, Ding YY, Leung BP, et al. Sex-specific differences in risk factors for sarcopenia amongst community-dwelling older adults. *Age (Omaha)*. 2015;37(6):121. doi:[10.1007/s11357-015-9860-3](https://doi.org/10.1007/s11357-015-9860-3)
70. Hooijmans MT, Niks EH, Burakiewicz J, et al. Non-uniform muscle fat replacement along the proximodistal axis in Duchenne muscular dystrophy. *Neuromuscul Disord*. 2017;27(5):458-464. doi:[10.1016/j.nmd.2017.02.009](https://doi.org/10.1016/j.nmd.2017.02.009)
71. Schlaffke L, Rehmann R, Froeling M, et al. Diffusion tensor imaging of the human calf: variation of inter- and intramuscle-specific diffusion parameters. *J Magn Reson Imaging*. 2017;46(4):1137-1148. doi:[10.1002/jmri.25650](https://doi.org/10.1002/jmri.25650)

**How to cite this article:** Jerban S, Shaterian Mohammadi H, Athertya JS, et al. Significant age-related differences between lower leg muscles of older and younger female subjects detected by ultrashort echo time magnetization transfer modeling. *NMR in Biomedicine*. 2024;37(12):e5237. doi:[10.1002/nbm.5237](https://doi.org/10.1002/nbm.5237)